

# Synchrotron Radiation-based X-ray phase-contrast imaging of the aortic walls in acute aortic dissection

Koki Yokawa, MD,<sup>a</sup> Masato Hoshino, PhD,<sup>b</sup> Naoto Yagi, PhD,<sup>b</sup> Yutaka Nakashima, MD, PhD,<sup>c</sup> Kazunori Nakagawa, PhD,<sup>d</sup> Yutaka Okita, MD, PhD,<sup>a</sup> Kenji Okada, MD, PhD,<sup>a</sup> and Takuro Tsukube, MD, PhD,<sup>a,e</sup> Kobe, Hyogo, and Fukuoka, Japan

## ABSTRACT

**Objective:** Synchrotron radiation-based X-ray phase-contrast tomography (XPCT) imaging is an innovative modality for the quantitative analysis of three-dimensional morphology. XPCT has been used in this study to evaluate ascending aorta specimens from patients with acute type A aortic dissection (ATAAD) and to analyze the morphologic structure of the aortic wall in patients with this condition.

**Methods:** Aortic specimens from 12 patients were obtained during repairs for ATAAD and were fixed with formalin. Five patients had Marfan syndrome (MFS), and seven did not. In addition, six normal aortas were obtained from autopsies. Using XPCT (effective pixel size, 12.5  $\mu\text{m}$ ; density resolution, 1  $\text{mg}/\text{cm}^3$ ), the density of the tunica media (TM) in each sample was measured at eight points. The specimens were subsequently analyzed pathologically.

**Results:** The density of the TM was almost constant within each normal aorta (mean,  $1.081 \pm 0.001 \text{ g}/\text{cm}^3$ ). The mean density was significantly lower in the ATAAD aortas without MFS ( $1.066 \pm 0.003 \text{ g}/\text{cm}^3$ ;  $P < .0001$ ) and differed significantly between the intimal and adventitial sides ( $1.063 \pm 0.003$  vs  $1.074 \pm 0.002 \text{ g}/\text{cm}^3$ , respectively;  $P < .0001$ ). The overall density of the TM was significantly higher in the ATAAD aortas with MFS than those without MFS ( $1.079 \pm 0.008 \text{ g}/\text{cm}^3$ ;  $P = .0003$ ), and greater variation and markedly different distributions were observed in comparison with the normal aortas. These density variations were consistent with the pathologic findings, including the presence of cystic medial necrosis and malalignment of the elastic lamina in the ATAAD aortas with and without MFS.

**Conclusions:** XPCT exhibited differences in the structure of the aortic wall in aortic dissection specimens with and without MFS and in normal aortas. Medial density was homogeneous in the normal aortas, markedly varied in those with MFS, and was significantly lower and different among those without MFS. These changes may be present in the TM before the onset of aortic dissection. (JVS—Vascular Science 2020;1:81-91.)

**Keywords:** Synchrotron Radiation-based X-ray Phase-Contrast Imaging; Aorta; Acute type A aortic dissection, tissue density

Surgical mortality for acute type A aortic dissection (ATAAD) has improved<sup>1</sup>; however, across all patients with aortic dissection, pre-hospital and pre-surgical

mortality remains a more than 60%.<sup>2</sup> To improve the overall survival rate of patients with ATAAD, it is crucial to establish the pathogenesis of ATAAD and a means of predicting this condition.<sup>3</sup>

X-ray phase-contrast tomography (XPCT) using synchrotron radiation (SR) is superior to conventional computed tomography (CT) scans and magnetic resonance imaging owing to its high resolution. The high sensitivity of phase-contrast imaging allows for the visualization of small density differences in biological soft tissue.<sup>4,5</sup> An SR-based XPCT that uses a Talbot grating interferometer has been developed at the Japan Synchrotron Radiation Research Institute/SPring-8, achieving a density resolution better than 1  $\text{mg}/\text{cm}^3$ .<sup>3</sup> Moreover, it has been used for the visualization of several soft biological tissues.<sup>6-8</sup> In a previous study, we used SR-based XPCT to obtain two-dimensional and three-dimensional (3D) imaging of the aortic wall of an ATAAD patient with Marfan syndrome (MFS).<sup>9</sup> This finding suggests that XPCT may be useful for the investigation of the morphologic characteristics of aortic diseases.

From the Division of Cardiovascular Surgery, Kobe University Graduate School of Medicine, Kobe<sup>a</sup>; the Research & Utilization Division, Japan Synchrotron Radiation Research Institute/SPring-8, Sayo, Hyogo<sup>b</sup>; the Division of Pathology, Japanese Red Cross Fukuoka Hospital,<sup>c</sup> and the Pathophysiological and Experimental Pathology, Graduate School of Medical Sciences, Kyushu University,<sup>d</sup> Fukuoka; and the Division of Cardiovascular Surgery, Japanese Red Cross Kobe Hospital, Kobe.<sup>e</sup>

Supported by Japan Society for the Promotion of Science, Grant Number 17K10754.

Author conflict of interest: none.

Correspondence: Kenji Okada, MD, PhD, Division of Cardiovascular Surgery, Kobe University Graduate School of Medicine, 7-5-2 Kusunokicho, Chuo-ku, Kobe, Japan 651-0073 (e-mail: [kokada@med.kobe-u.ac.jp](mailto:kokada@med.kobe-u.ac.jp)).

The editors and reviewers of this article have no relevant financial relationships to disclose per the JVS-Vascular Science policy that requires reviewers to decline review of any manuscript for which they may have a conflict of interest.

2666-3503

Copyright © 2020 by the Society for Vascular Surgery. Published by Elsevier Inc.

This is an open access article under the CC BY-NC-ND license (<http://creativecommons.org/licenses/by-nc-nd/4.0/>).

<https://doi.org/10.1016/j.jvssci.2020.06.002>

The present study aimed to investigate structural changes in the aortic wall of a patient with ATAAD using XPCT through detailed visualization and structural quantification.

## METHODS

**Aorta specimens.** Specimen collection was approved by the Institutional Review Board of the Japanese Red Cross Kobe Hospital, and informed consent was obtained from all patients. The investigation conformed to the principles outlined in the Declaration of Helsinki. Rings from the dissected ascending aortas were freshly obtained from ATAAD patients ( $n = 12$ ; 10 men and 2 women; 5 with MFS) who underwent emergent aortic replacement at the Japanese Red Cross Kobe Hospital. Each specimen was a 2-cm-wide transverse aortic ring collected 3 cm above the sinotubular junction of the ascending aorta. The specimens were fixed with 10% formalin; then, 3D images were obtained, and densitometric analysis was performed within 6 months by XPCT. In addition, six formalin-fixed normal ascending aortas were obtained from autopsies (five from men). No significant differences were observed in terms of patient age among the three types of specimen. The mean age of patients with MFS was  $44.8 \pm 15.1$  years, patients without MFS,  $56.9 \pm 8.9$  years, and patients with normal aortas,  $58.0 \pm 4.9$  years. Patient characteristics are presented in Table 1. One representative aortic sample with chronic aortic dissection was added to demonstrate the degree of contribution of elastic fibers to the density of the XPCT image.

**XPCT imaging.** Fig 1 presents a schematic diagram of the XPCT system in the SPring-8 SR facility that was based on an X-ray Talbot grating interferometer in the bending-magnet synchrotron beamline. The system has been described in detail elsewhere.<sup>6,7</sup> Briefly, the system was located 200 m from an X-ray source and tuned to 25 keV by passing it through a silicon double-crystal monochromator. The specimen was placed in an appropriately sized plastic canister filled with saline and rotated slowly in the canister with a rotating stage. The Talbot grating interferometer that comprised phase grating and absorption grating was placed behind the specimen, and moiré fringes generated by the interferometer were detected using an X-ray detector (Fig 1, A). Phase retrieval was achieved using a five-step phase-stepping procedure that involved shifting of the absorption grating with a piezo-driven stage (Fig 1, B). The data were processed using a high-throughput system to create 3D images, and the system specifications were as follows: field of view, 24.7 mm (H)  $\times$  17.1 mm (V); voxel size, 12.5  $\mu\text{m}$ ; spatial resolution, 25  $\mu\text{m}$ ; density resolution, 1  $\text{mg}/\text{cm}^3$ ; exposure time, 1 s/image; and number of projections, 900. The horizontal field of view (ie, the field of view in the reconstructed slice image) could be extended by up to 40 mm by using an offset tomographic scan. The density is

## ARTICLE HIGHLIGHTS

- **Type of Research:** Basic science research.
- **Key Findings:** In acute aortic dissection, the density of the tunica media of the aortic wall was significantly lower and differed between the intimal and adventitial sides compared with the aortic wall of the normal aorta.
- **Take Home Message:** The structure of the aortic wall in acute aortic dissection was different from that of the aortic wall of the normal aorta.

proportional to the amount of phase shift per voxel that can be reconstructed using the data from the X-ray phase tomography. This is the same process by which conventional CT provides a Hounsfield unit value of a voxel. Moreover, X-ray phase tomography has a much higher sensitivity for biological soft tissues than conventional CT (Fig 2). This is because the image contrast obtained from X-ray phase tomography is based on the phase shift of the X-ray as an electromagnetic wave passing through the specimen, whereas image contrast in conventional CT is based on the X-ray amplitude attenuation. A physical quantity that is about 1000 times larger than that in the attenuation is involved in the phase shift; thus, in principle, X-ray phase tomography has a high sensitivity for soft tissues.<sup>5,6</sup> The ability to visualize small differences in density and fine details in the structure is attributable to high spatial and density resolution.<sup>8</sup>

The reconstructed volumes were converted into 16-bit TIFF images of each tomography slice with custom-made original software. Further image processing and analysis of the tomography data were performed using the ImageJ software (<http://rsbweb.nih.gov/ij/index.html>).<sup>6,7</sup> Morphologic differences were quantitatively evaluated by estimating the mean mass density of the TM within eight regions of interest in the aortic wall of each formalin-fixed sample. Each region of interest was  $150 \times 150 \times 10$  voxels.

**Histologic examinations.** After completion of XPCT imaging, the samples were stored in 10% formalin and sectioned transversely. Thereafter, the sections of each specimen were stained with hematoxylin and eosin, elastica van Gieson (EVG), Picrosirius red, and Alcian blue stains. The EVG, Picrosirius red, and Alcian blue stains were used to detect elastic fibers, collagen fibers, and acid mucopolysaccharide, respectively. Smooth muscle cells (SMCs) were identified by immunostaining with anti- $\alpha$ -smooth muscle actin antibody (DAKO, Denmark A/S, Glostrup, Denmark). The histologic examination focused on the identification of cystic medial necrosis (CMN), laminar medial necrosis, atherosclerosis, fibrosis of the media, and any changes to the vasa vasorum. CMN was defined as the focal fragmentation and/

**Table I.** Patient characteristics of acute aortic dissection with Marfan syndrome (MFS), without MFS (Non-MFS), and normal aortas

	MFS	Non-MFS	Control	P value
Patients	5	7	6	
Age, years	44.8 ± 15.1	56.9 ± 8.9	58.0 ± 5.0	NS
Sex, male	5	5	4	NS
Hypertension	1	4	0	NS
Coronary arterial disease	0	1	0	NS
CT findings				
Normal aorta	0	0	6	
Location of intimal tear				
Ascending aorta	3	3		NS
Aortic arch	2	4		
Patent false lumen	5	5		NS
Procedures				
Total arch replacement	4	4	N/A	
Hemi-arch replacement	1	3	N/A	

CT, Computed tomography; N/A, not applicable; NS, not significant. Values are number or mean ± standard deviation.

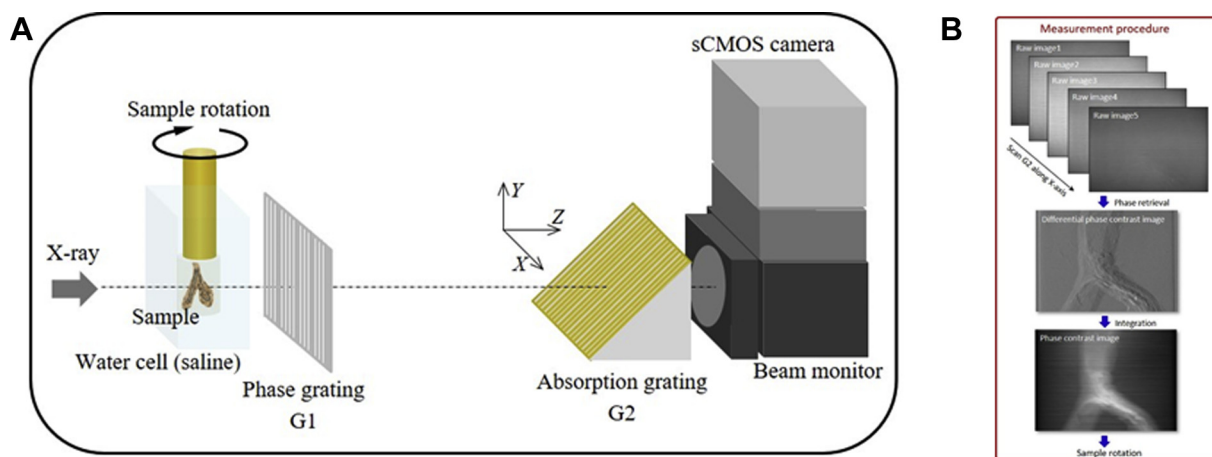


**Fig 1.** Schematic diagram of the experimental setup for the X-ray phase-contrast (XPCT) imaging. Schematic drawing of the experimental setup for the XPCT imaging based on the grating interferometer. **A**, A Talbot grating interferometer, consisting of phase grating and absorption grating, was placed behind the specimen. **B**, Phase retrieval was achieved using a five-step phase-stepping procedure. sCMOS, Scalable complementary metal-oxide semiconductor.

or loss of elastic fibers and SMCs in the media associated with deposits of various amounts of acid mucopolysaccharide and/or fibrous tissue. If the CMN amount was small, multifocal lesions were regarded as a positive finding. Lamellar medial necrosis was defined as lamellar or band-like loss of the media's SMCs.<sup>10</sup>

Moreover, to evaluate the contribution of elastic fibers to the densitometric changes in the TM, the occupation ratio of the aortic components, such as elastic fibers, collagen fibers, and SMCs, was determined in a chronic aortic dissection sample. The occupation ratio was defined as the percentage of the area occupied by

each aortic component to the selected area. This sample had a region where the occupation ratio of collagen was almost the same as that in the TM, and elastic fibers were rare; Fig 3 demonstrates that three areas, size 500 × 500 μm square, were selected and named area 1 in the TM, area 2 in the organized thrombus composed of fibrocellular tissue, and area 3 in the tunica adventitia affected by fibrosis. Then, the occupation ratio of elastic fibers, collagen fibers, and SMCs in each area was morphologically analyzed by an experienced pathologist (Y.N.) using Adobe Photoshop (San Jose, Calif) and compared with the mass density of the same area in the XPCT image in Table II.

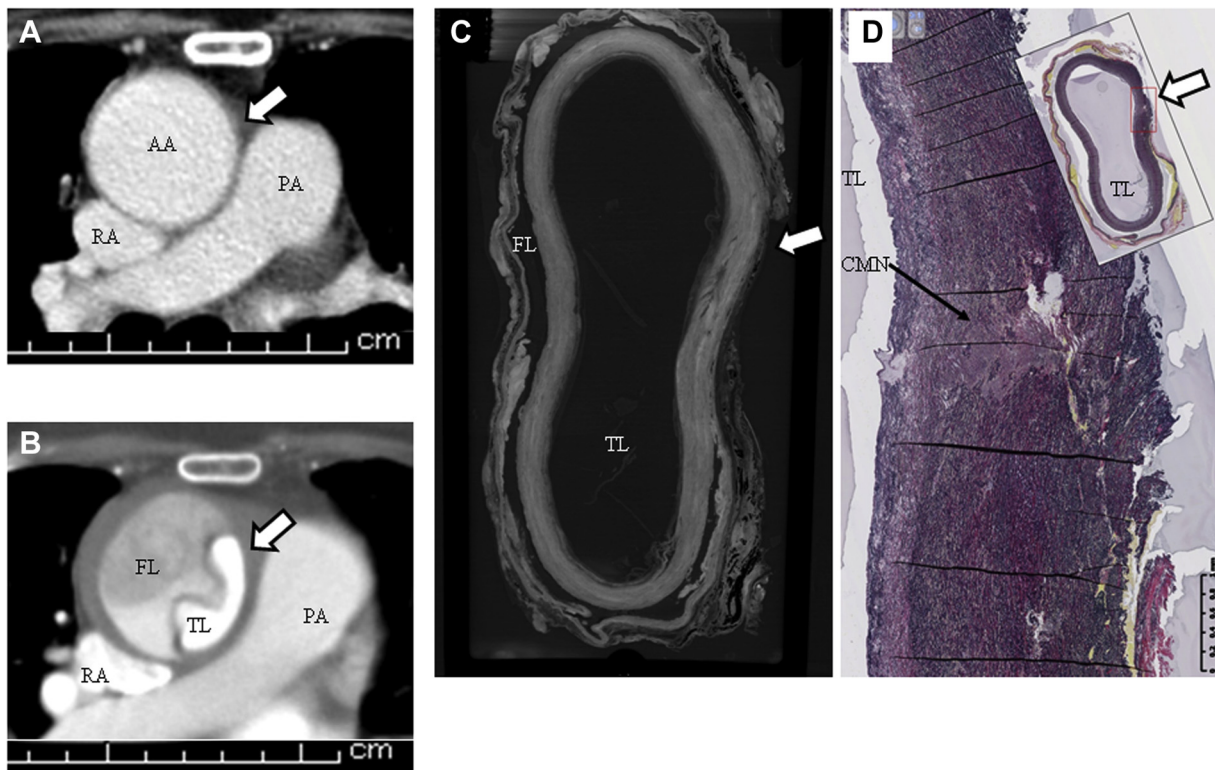


**Fig 2.** Clinical and laboratory imaging findings from patient 1. **A**, A contrast-enhanced computed tomography (CT) scan obtained 3 years before the onset of acute aortic dissection type A, showing thin and even image contrast of the aortic wall (arrow). **B**, A contrast-enhanced CT scan at the onset of acute aortic dissection type A, showing the true lumen and the false lumen of the ascending aorta without significant changes in the aortic wall (arrow). **C**, An X-ray phase-contrast tomography (XPCT) image of the same slice of the aortic wall, showing density variation in the tunica media (TM) (arrow). **D**, Pathologic findings in a specimen stained with elastica van Gieson (EVG) stain that clearly demonstrated tears in the elastic lamina and cystic medial necrosis (CMN; black arrow). AA, Ascending aorta; PA, pulmonary artery; RA, right atrium; TL, true lumen; FL, false lumen; LV, left ventricle; RV, right ventricle.

**Statistical analyses.** All statistical tests were conducted using the JMP statistical software (SAS Institute, Cary, North Carolina). Student's *t* tests were used to compare the densities in the TMs of the aortas. Statistical significance was set at a *P* value of less than .05. Data are expressed as mean  $\pm$  standard deviation.

## RESULTS

**Representative conventional CT and XPCT images.** Conventional CT images of a 67-year-old woman before and at the onset of ATAAD (Fig 2, A and B, respectively) exhibited a thin image contrast of the ascending aortic wall. The XPCT imaging of the same slice clearly demonstrated density variation in the TM (Fig 2, C). This corresponded with CMN and elastic lamina malalignment (Fig 2, D).

**Representative mass density and occupation ratio of the aortic components.** The mass density and occupation ratio of the elastic fiber were markedly increased in area 1 compared with area 2, whereas the ratio of

collagen fiber was similar in both the areas of a representative aortic sample with chronic aortic dissection (Fig 3). This suggests that the density in the XPCT image in the TM in aortic dissection is mainly determined by elastic fibers (Table II).

**Quantitative assessment of the tunica media of the aorta.** To quantitatively evaluate the morphologic differences, the tunica media (TM) densities were estimated in each sample. In the normal aortas ( $n = 6$ ), the mean density of the TM was  $1.081 \pm 0.001$  (range, 1.075–1.087  $\text{g}/\text{cm}^3$ ), and there was no significant variation within the TM. Fig 4, A and B, presents an XPCT image of a normal aorta and a specimen stained with EVG stain. A histogram of the density map revealed a high peak at a density of around  $1.081 \text{ g}/\text{cm}^3$  (Fig 4, C). A line profile of the density from the intima to the adventitia showed that the medial density remained unchanged between the inner and outer media at around  $1.080 \text{ g}/\text{cm}^3$  (Fig 4, D). These findings were consistent with the histologic findings for the same region, wherein uniform

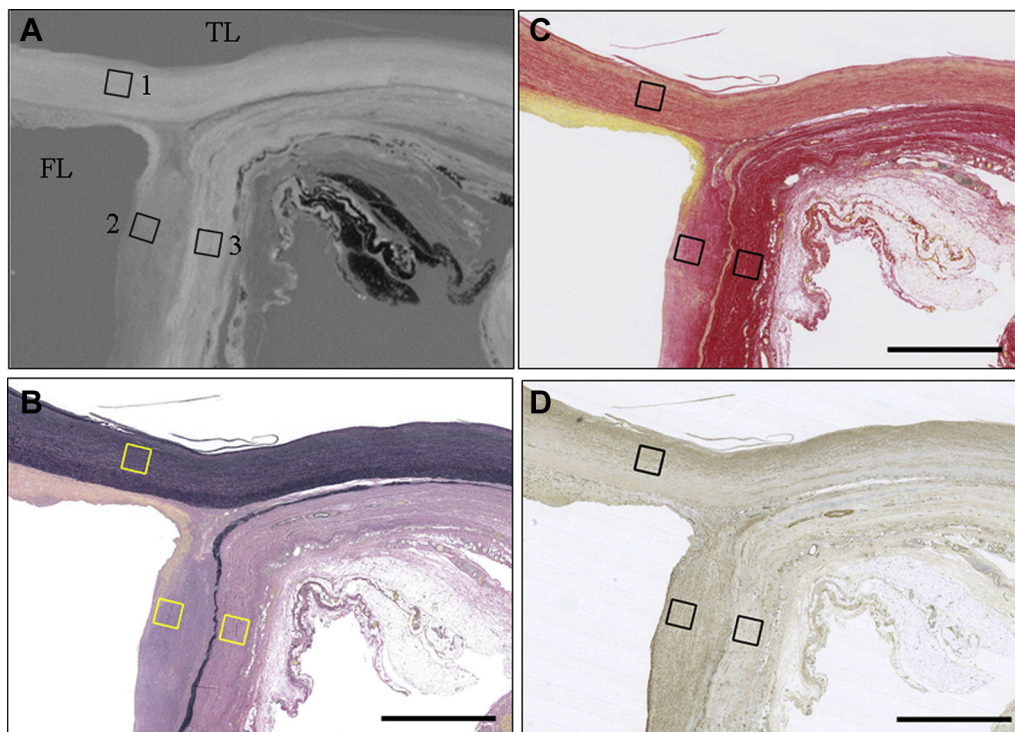


**Fig 3.** The relationship between the X-ray phase-contrast tomography (XPCT) image and aortic components. **A,** An XPCT image. **B,** Elastica van Gieson (EVG) stain. **C,** Picrosirius red stain. **D,** Smooth muscle cells (SMCs). The three squares in each panel indicate the areas where the density in the XPCT image and the percentage of the area occupied (occupation ratio) by elastic fibers, collagen fibers, and SMCs were determined. Three areas, size  $500 \times 500 \mu\text{m}$  square, were selected. Area 1, Area 2, and Area 3 are the representative areas of the aortic media, organized thrombus in the false lumen, and adventitia affected by fibrosis, respectively. TL, True lumen; FL, false lumen. Bars = 2.5 mm.

**Table II.** Comparison of the density in the X-ray phase-contrast tomography (XPCT) image and occupation ratio of aortic components of the corresponding areas in the aortic wall of a representative aortic sample with chronic aortic dissection

Area	Density in the XPCT image, g/cm <sup>3</sup>	Occupation ratio (%)			
		Elastic fibers	Thin and discretely arranged collagen fibers	Thick and densely arranged Collagen fibers	SMCs
1	$1.073 \pm 0.004$	71.1	47.9		19.9
2	$1.0324 \pm 0.004$	0.2	44.9		17.4
3	$1.0744 \pm 0.008$	4.4		90.3	4.9

*Occupation ratio, Percentage of the area occupied by each aortic component to the selected area; SMCs, smooth muscle cells.*

high-density elastic fibers were observed in the media (Fig 4, B). These findings may show that the density of the media of the normal aorta is homogeneous, providing the vessels with a stable structure.

In the specimens of the ATAAD without MFS ( $n = 7$ ), the mean density of the TM of the undissected portion of the aorta was  $1.066 \pm 0.003 \text{ g/cm}^3$  (range,  $1.052\text{--}1.074 \text{ g/cm}^3$ ), which was significantly lower than the density in the normal aortas ( $P < .0001$ ). Moreover, a significant difference was observed in the density of the inner and outer media ( $1.063 \pm 0.003$  vs  $1.074 \pm 0.002$ , respectively;  $P < .0001$ ). Fig 5, A and B,

presents an XPCT image and a stained specimen. A histogram of the density of the TM in an undissected portion of the sample revealed two broad peaks at around  $1.03$  and  $1.07 \text{ g/cm}^3$  (Fig 5, C). A line profile of the density from the intima to the adventitia showed that the medial density exhibited considerable variation, in the range of  $1.02$  to  $1.09 \text{ g/cm}^3$ , and was higher in the outer media than in the inner media (Fig 5, D). The XPCT findings were consistent with the histologic findings, including the presence of CMN and the difference in the density of elastic fibers between the inner and outer media (Fig 5, B).

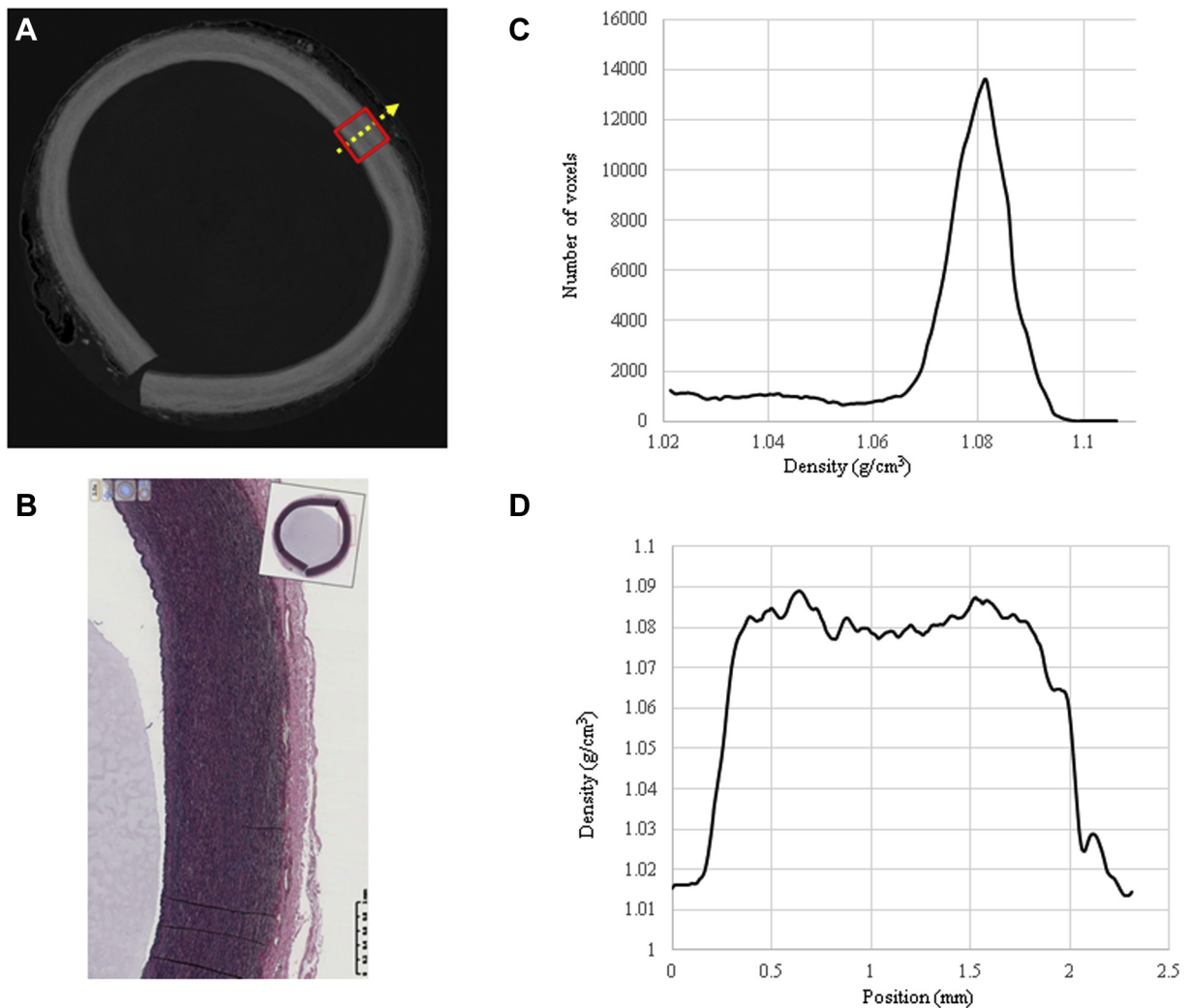


**Fig 4.** A representative X-ray phase-contrast tomography (XPCT) image and histologic findings in normal aortas. **A**, A representative two-dimensional XPCT image of the normal aorta. A red square, size  $150 \times 150$  voxels, was selected in the tunica media (TM), and a yellow arrow was determined for a line profile of the density in the TM. **B**, A normal aorta stained with elastica van Gieson (EVG) stain. **C**, A histogram of the density map in the TM of the sample (indicated by the red square in **A**) exhibited a high peak at a density of around  $1.081 \text{ g/cm}^3$ . **D**, A line profile of the density from the intima to the adventitia (indicated by the yellow arrow in **A**) showed that the density remained unchanged between the inner and outer media at around  $1.080 \text{ g/cm}^3$ .

In the samples from patients with ATAAD with MFS ( $n = 5$ ), the mean density of the TM of the undissected portions was  $1.079 \pm 0.008 \text{ g/cm}^3$  (range,  $1.069\text{--}1.084 \text{ g/cm}^3$ ), which was significantly higher than the density in the ATAAD aortas without MFS ( $P = .0003$ ). Fig 6, A and B, presents an XPCT image and a stained specimen. The histogram of the density map reveals right deviation of the bimodal peaks of density (Fig 6, C). A line profile of the density from the intima to the adventitia showed a continuous change in the medial density, in the range of  $1.04$  to  $1.10 \text{ g/cm}^3$ , and the density was higher in the inner media than in the outer media (Fig 6, D). The XPCT findings were consistent with the histologic findings, including the presence of CMN and the difference in the density of elastic fibers between the inner and outer media (Fig 6, B). Fig 7

presents the histologic findings of CMN. Elastic fibers, collagen fibers, and SMCs were lost or decreased, and ground substances (acid mucopolysaccharide) accumulated in the lesion. Structural weakness of the media was suspected with qualitative information obtained from these different stains. Meanwhile, XPCT indicated the change in the media with quantitative values. The density of CMN was  $1.037 \text{ g/cm}^3$ , which was markedly lower than that of the surrounding tissue (Fig 6, D).

Fig 8 presents the density histograms for the following three types of aorta: ATAAD with MFS, ATAAD without MFS, and normal aorta. This clearly demonstrates the significant differences among the three types. In the ATAAD and MFS aortas, the density of the TM exhibited lower

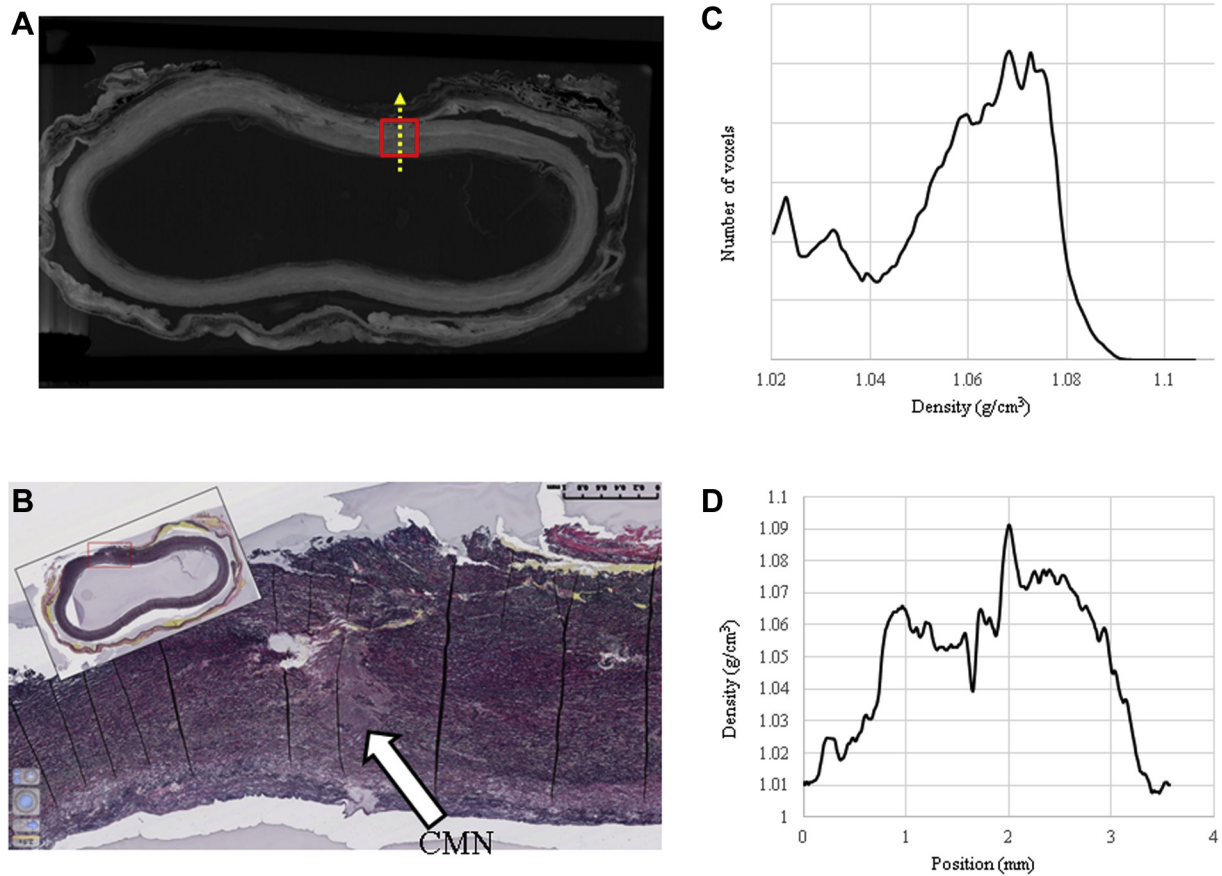


**Fig 5.** A representative X-ray phase-contrast tomography (XPCT) image and histologic findings in the aortas of the patients with acute aortic dissection type A. **A**, A representative two-dimensional XPCT image of a dissecting aorta. A *red square*, size  $150 \times 150$  voxels, was selected in the tunica media (TM), and a *yellow arrow* was determined for a line profile of the density in the TM. **B**, A specimen stained with elastica van Gieson (EVG) stain. The histologic findings were consistent with the XPCT findings, including the presence of cystic medial necrosis (CMN, *arrow*) and the difference in the density of the elastic fibers between the inner and outer media. **C**, A histogram of the density map in the TM of an undissected portion of the sample (indicated by the *red square* in **A**) exhibiting dispersed density with peaks at densities of around  $1.03$  and  $1.07$   $\text{g}/\text{cm}^3$ . **D**, A line profile of the density from the intima to the adventitia (indicated by the *yellow arrow* in **A**) showed continuous variation.

and wider dispersion with bimodal peaks compared with the single peak observed in the normal aortas. The density of the TM of the MFS aortas was significantly higher than that of the ATAAD aortas without MFS ( $P = .0003$ ).

## DISCUSSION

SR-based XPCT has been used successfully for the visualization of the microstructure of normal and pathologic tissues, including the lungs,<sup>11</sup> brain,<sup>5</sup> eyes,<sup>12</sup> heart,<sup>13</sup> and, more recently, the aorta<sup>9</sup> and a whole human fetus heart.<sup>14</sup> In principle, SR-based XPCT is about 1000 times more sensitive in detecting light elements than conventional X-ray absorption-contrast techniques.<sup>8</sup> Further, SR-based XPCT has the following three major advantages: it enables quantitative analyses of the densities of the microstructures of various soft tissues, facilitating quantitative comparisons

among many different types of soft tissues; it allows for the visualization of tissue microstructures and mass density without using contrast agent; and it provides high-resolution and 3D images without destroying or altering the properties of the specimens.<sup>5,6,11</sup> The gold standard to obtain information of the soft tissue is histology, a destructive and labor-intensive technique where the specimen is sliced and examined under a light microscope.<sup>15</sup> In addition, regions of interest cannot be located beforehand and the analysis is intrinsically two-dimensional.<sup>15</sup> To overcome the limitations of conventional histology, XPCT has been applied for various soft tissues, and these works show that XPCT can be used to perform noninvasive 3D virtual histology on unstained formalin-fixed human tissues at high resolution, allowing for quantification of tissue structures as well as the localization of small regions of interest.<sup>7,14,16,17</sup>

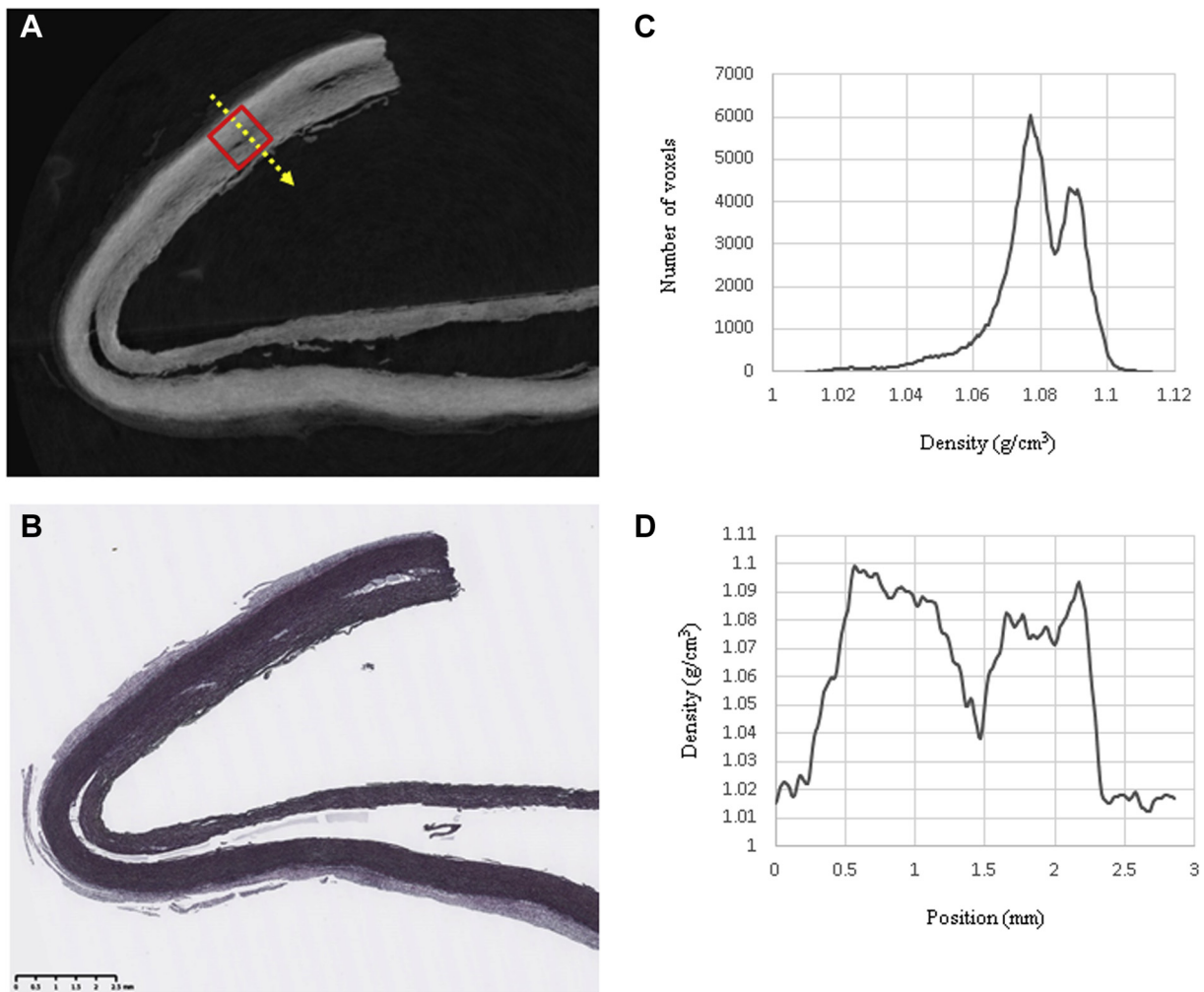


**Fig 6.** A representative X-ray phase-contrast tomography (XPCT) image and histologic findings in the aortas of the patients with acute aortic dissection and Marfan syndrome (MFS). **A**, A representative two-dimensional XPCT image of a dissecting aorta. A *red square*, size  $150 \times 150$  voxels, was selected in the tunica media (TM), and a *yellow arrow* was determined for a line profile of the density in the TM. **B**, A specimen stained with elastica van Gieson (EVG) stain. The histologic findings were consistent with the XPCT findings, including the presence of cystic medial necrosis (CMN) and the difference in the density of the elastic fibers between the inner and outer media. **C**, A histogram of the density map in the TM of an undissected portion of the sample (indicated by the *red square* in **A**) exhibiting two gentle peaks between 1.06 and 1.1  $\text{g}/\text{cm}^3$ . **D**, A line profile of the density from the intima to the adventitia (indicated by the *yellow arrow* in **A**) showed that the medial density was constantly changing.

In the present study, we conducted a quantitative comparison of several types of aortic walls that exhibited differences in the microstructure of the aortic wall between specimens from patients with aortic dissection and those with a normal aorta. The tissue density in the TM of the normal ascending aortas was almost homogeneous, with a single peak in the density histogram at approximately  $1.080 \text{ g}/\text{cm}^3$ . The aortas of patients with ATAAD but without MFS exhibited a significantly lower density of the TM ( $1.066 \pm 0.003 \text{ g}/\text{cm}^3$ ), with the density histogram for the undissected portion of the ascending aorta showing a dispersed distribution with two peaks. The differences in the mass density between the normal and the ATAAD without MFS aorta were consistent with

the distribution of elastic fibers observed in the corresponding histologic samples. The dissecting aortas without MFS exhibited the presence of CMN and differences in the density of elastic fibers between the inner and outer media. These findings are consistent with previous studies, wherein the elastin concentration in the ascending aortas with aortic dissection was significantly lower than that in the normal aortas,<sup>18,19</sup> and a decrease in the overall elastic content and elastic concentration in the interlamellar fibers was reported.<sup>20,21</sup> Whereas, the specimens from patients with ATAAD with MFS exhibited a higher density that was not significantly different from that in the normal aortas. However, the density distribution was not homogeneous, and the

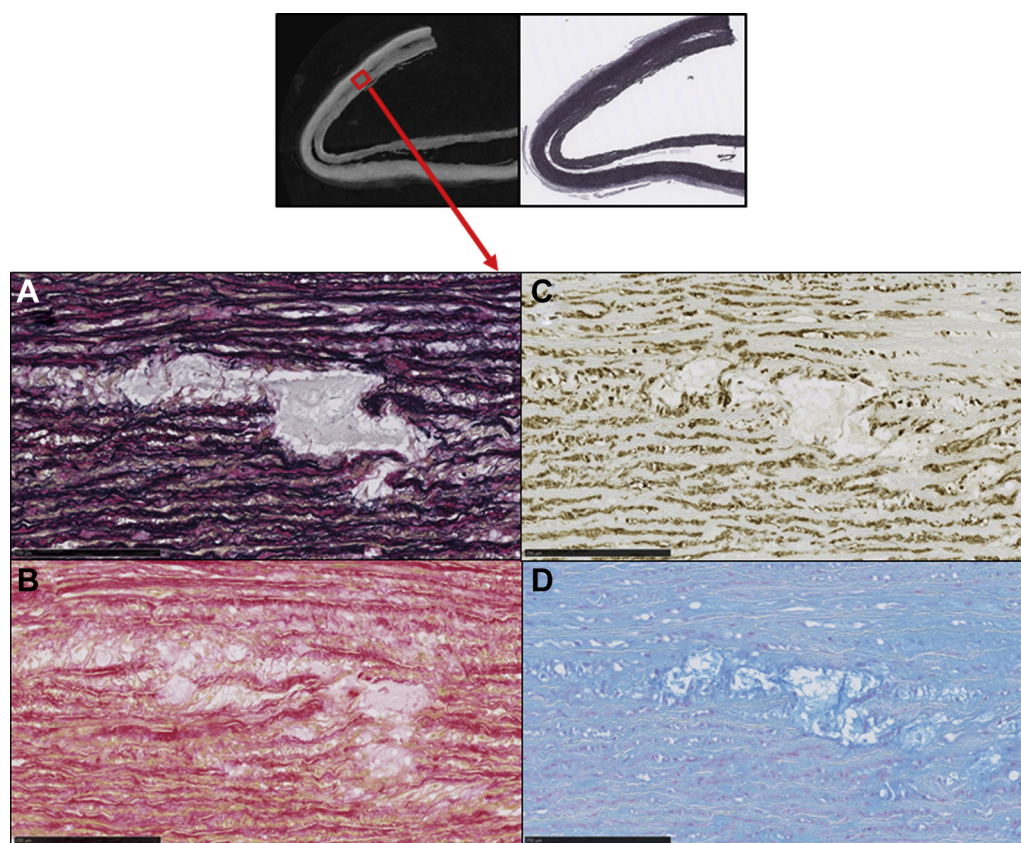


**Fig 7.** A representative X-ray phase-contrast tomography (XPCT) image and histologic findings of cystic medial necrosis (CMN). CMN lesions in the XPCT image (*red square*) indicate focal loss or decrease in the elastic fibers (**A**), collagen fibers (**B**), smooth muscle cells (SMCs) (**C**), and deposits of acid mucopolysaccharide (**D**). **A**, Elastica van Gieson (EVG) stain. **B**, Picosirius red stain. **C**, Immunohistochemistry using anti- $\alpha$ -smooth muscle actin. **D**, Alcian blue stain. Bars represent 250  $\mu\text{m}$ .

histogram showed a bimodal peak at a density of approximately  $1.079 \text{ g/cm}^3$ . These differences in the density distribution of the TM correspond with the differences in the pathologic findings that have been previously reported.<sup>22,23</sup>

This study demonstrated that SR-based XPCT is an innovative modality for the analysis of 3D morphology and is useful for understanding the pathophysiology of various cardiovascular diseases. Currently, the quality of the densitometric data of the aortic wall is high enough to visualize and automatically locate regions of interest, such as CMN, within the TM of ATAAD, and to provide 3D virtual histology of the various aortic pathologies. However, the application of XPCT has been limited to the clinical level, and there are certain problems that need to be solved if used for in vivo human aorta imaging. The bones of the chest wall around the aorta are a major barrier. Because XPCT makes it possible to visualize soft tissue structures by rendering phase shifts in the X-rays visible, phase retrieval in XPCT does not remove the artefacts from the highly absorbing bones around the tissue and from imperfections in the imaging system that can obscure those structures. In comparison, recent study showed development of in situ phase

contrast X-ray brain CT scans, demonstrating its high stability in the presence of noise from bone of the skull.<sup>24</sup> Another potential barrier is a radiation dose to the human body. High-dose radiation is required to achieve high-density resolution and spatial resolution. In this study, the radiation dose is approximately 14 mSv/s and exposed dose may exceed 50 Sv for one-time measurement. However, the X-ray phase imaging concept is being translated into hospitals, and recent approaches using a grating interferometer have permitted the use of conventional X-ray sources in the fields of joint disease and breast cancer.<sup>25,26</sup> Thus, the XPCT system has the possibility to be developed for in vivo imaging of the human aorta.

This study has certain limitations. First, the density in the XPCT image includes all of the aortic components. Elastin and collagen are key fibrous proteins that are found in the arterial walls. Findings from a representative sample of patients with chronic aortic dissection suggested that mass density in the XPCT image in the TM in aortic dissection may be mainly determined by elastic fibers (Fig 3; Table II). However, applying this analysis on the samples of acute aortic dissection is challenging, because it is difficult to find a region where the

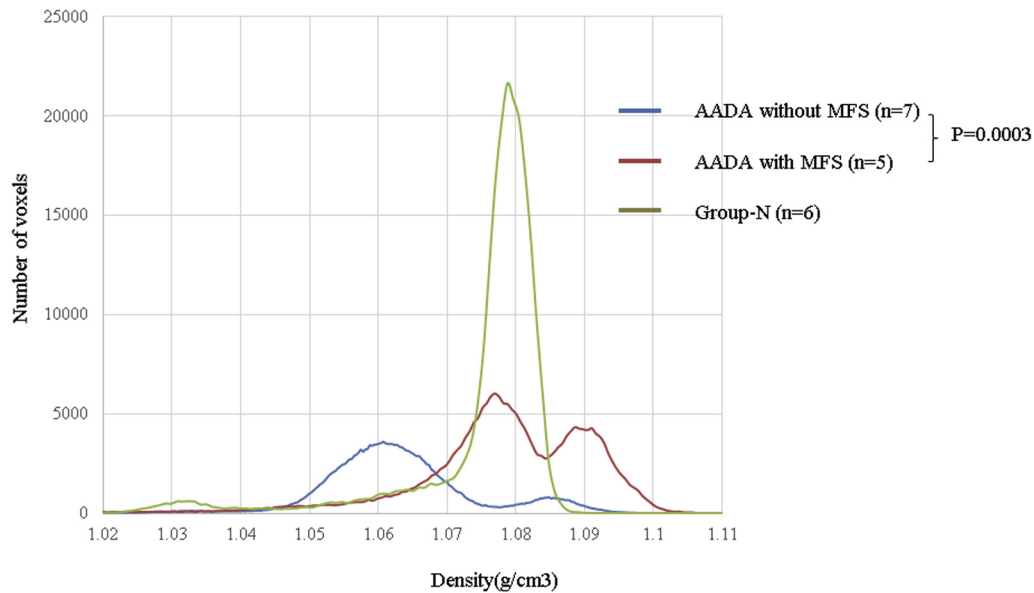


**Fig 8.** Comparison of the density histograms of the three types of aortas: acute aortic dissection type A with and without Marfan syndrome (MFS) and intact aorta.  $P = .0003$ . AADA, Acute type A aortic dissection.

occupation ratio of collagen is similar to that in the TM and where elastic fibers are rare. Second, the sample size was 18 and relatively small; however, the XPCT analysis was conducted rigorously, with eight aortic sections selected per patient and a total of 144 regions analyzed. Third, the patients were limited to those aged less than 70 years. There is an established connection between aging and atherosclerosis and calcification.<sup>27</sup> However, calcified samples are unsuitable for XPCT imaging; therefore, specimens from older patients were not investigated. Fourth, all the samples were collected from the same area of the ascending aorta. However, considering the heterogeneity along the aorta, further studies may be needed to examine the aorta at varying sites.

## CONCLUSIONS

SR-based XPCT imaging is a valuable modality for understanding the aortic structures and morphologic changes in aortic dissection. The structure of the aortic wall differed significantly between the samples from patients with AADA with and without MFS and those from subjects with intact aortas. These degenerations occurred before the onset of aortic dissection.

This study was approved by the Japanese Red Cross Kobe Hospital Research Subjects Review Boards and SPring-8 Proposal Review Committee (2015A1581, 2015B1491, 2016A1186). The authors thank Kimito Minami MD, PhD for statistical advices, and Kyoichi Ogawa MD, Akio Yamanaka MD, Katsuhiko Nakamae PhD and members of the SPring 8 Cardiovascular Structure Analyzing Research Group for giving insightful comments and suggestions.

## AUTHOR CONTRIBUTIONS

Conception and design: KY, MH, YN, YO, KO, TT

Analysis and interpretation: KY, MH, NY, YN, KN, TT

Data collection: KY, MH, NY, YN, KN, TT

Writing the article: KY, TT

Critical revision of the article: KY, MH, NY, YN, KN, YO, KO, TT

Final approval of the article: KY, MH, NY, YN, KN, YO, KO, TT

Statistical analysis: KY, TT

Obtained funding: TT

Overall responsibility: KO

## REFERENCES

1. Committee for Scientific Affairs, The Japanese Association for Thoracic Surgery, Masuda M, Okumura M, Doki Y, Endo S, Hirata Y, Kobayashi J, et al. Thoracic and cardiovascular surgery in Japan during 2014. Annual report by The Japanese Association for Thoracic Surgery. *Gen Thorac Cardiovasc Surg* 2016;64:665-97.
2. Murai T, Baba M, Ro A, Murai N, Matsuo Y, Takada A, et al. Sudden death due to cardiovascular disorders: a review of the studies on the medico-legal cases in Tokyo. *Keio J Med* 2001;50:175-81.
3. Nakashima Y. Pathogenesis of aortic dissection: elastic fiber abnormalities and aortic medial weakness. *Ann Vasc Dis* 2010;3:28-36.
4. Margaritondo G, Meuli R. Synchrotron radiation in radiology: novel X-ray sources. *Eur Radiol* 2003;13:2633-41.
5. Momose A, Fukuda J. Phase-contrast radiographs of non-stained rat cerebellar specimen. *Med Phys* 1995;22:375-9.
6. Hoshino M, Uesugi K, Yagi N. Optimization of X-ray phase contrast imaging system toward high-sensitivity measurements of biological organs. *AIP Conf Proc* 2012;1466:255-60.
7. Hoshino M, Uesugi K, Tsukube T, Yagi N. Quantitative and dynamic measurements of biological fresh samples with

- X-ray phase contrast tomography. *J Synchrotron Rad* 2014;21:1347-57.
8. Tsukube T, Hoshino M, Yagi N. X-ray phase-contrast tomography opens new era for cardiovascular research. *Eur Heart J Cardiovasc Imag* 2017;18:742-3.
  9. Tsukube T, Yagi N, Hoshino M, Nakashima Y, Nakagawa K, Okita Y. Impact of synchrotron radiation-based X-ray phase-contrast tomography on understanding various cardiovascular surgical pathologies. *Gen Thorac Cardiovasc Surg* 2015;63:590-2.
  10. Nakashima Y, Kurozumi T, Sueishi K, Tanaka K. Dissecting aneurysm: a clinicopathologic and histopathologic study of 111 autopsied cases. *Hum Pathol* 1990;21:291-6.
  11. Yagi N, Suzuki Y, Umetani K, Kohmura Y, Yamasaki K. Refraction-enhanced X-ray imaging of mouse lung using synchrotron radiation source. *Med Phys* 1999;26:2190-3.
  12. Hoshino M, Uesugi K, Yagi N, Mohri S, Regini J, Pierscionek B. Optical properties of in situ eye lenses measured with X-ray Talbot interferometry: a novel measure of growth processes. *PLoS One* 2011;6:e25140.
  13. Zanette I, Bech M, Rack A, Le Duc C, Tafforeau P, David C, et al. Trimodal low-dose X-ray tomography. *Proc Natl Acad Sci U S A* 2012;109:10199-204.
  14. Kaneko Y, Shinohara G, Hoshino M, Morishita H, Morita K, Oshima Y, et al. Intact Imaging of human heart structure using x-ray phase-contrast tomography. *Pediatr Cardiol* 2017;38:390-3.
  15. Albers J, Pacilé S, Markus MA, Wiart M, Vande Velde G, Tromba G, et al. X-ray-based 3D virtual histology-adding the next dimension to histological analysis. *Mol Imaging Biol* 2018;20:732-41.
  16. Saccomano M, Albers J, Tromba G, Dobrovojević Radmilović M, Gajović S, Alves F, et al. Synchrotron inline phase contrast  $\mu$ CT enables detailed virtual histology of embedded soft-tissue samples with and without staining. *J Synchrotron Radiat* 2018;25:1153-61.
  17. Topperwien M, van der Meer F, Stadelmann C, Salditt T. Three-dimensional virtual histology of human cerebellum by X-ray phase-contrast tomography. *Proc Natl Acad Sci U S A* 2018;115:6940-5.
  18. Nakashima Y, Shiokawa Y, Sueishi K. Alterations of elastic architecture in human aortic dissecting aneurysm. *Lab Invest* 1990;62:751-60.
  19. Cattell MA, Hasleton PS, Anderson JC. Increased elastin content and decreased elastin concentration may be predisposing factors in dissecting aneurysms of human thoracic aorta. *Cardiovasc Res* 1993;27:176-81.
  20. Sariola H, Viljanen T, Luosto R. Histological pattern and changes in extracellular matrix in aortic dissections. *J Clin Pathol* 1986;39:1074-81.
  21. Nakashima Y, Sueishi K. Alteration of elastic architecture in the lathyrict rat aorta implies the pathogenesis of aortic dissecting aneurysm. *Am J Pathol* 1992;140:959-69.
  22. Osada H, Kyogoku M, Matsuo T, Kanemitsu N. Histopathological evaluation of aortic dissection: a comparison of congenital versus acquired aortic wall weakness. *Interact Cardio Vasc Thorac Surg* 2018;27:277-83.
  23. Grewal N, Gittenberger-de Groot AC. Pathogenesis of aortic wall complications in Marfan syndrome. *Cardiovasc Pathol* 2018;33:62-9.
  24. Croton CP, Morgan KS, Paganin DM, Kerr LT, Wallace MJ, Crossley KL, et al. In situ phase contrast X-ray brain CT. *Sci Rep* 2018;8:11412.
  25. Donath T, Pfeiffer F, Bunk O, Grünzweig C, Hempel E, Popescu S, et al. Toward clinical X-ray phase-contrast CT: demonstration of enhanced soft-tissue contrast in human specimen. *Invest Radiol* 2010;45:445-52.
  26. Momose A, Yashiro W, Kido K, Kiyohara J, Makifuchi C, Ito T, et al. X-ray phase imaging: from synchrotron to hospital. *Philos Trans A Math Phys Eng Sci* 2014;372:20130023.
  27. Tsamis A, Krawiec JT, Vorp DA. Elastin and collagen fibre microstructure of the human aorta in ageing and disease: a review. *J R Soc Interf* 2013;10:20121004.

Submitted Jan 9, 2020; accepted Jun 9, 2020.